TOPOLOGY OPTIMIZATION-GUIDED STIFFENING OF COMPOSITES REALIZED THROUGH AUTOMATED FIBER PLACEMENT

L. Esposito[1], A. Cutolo[1], M. Barile[2], L. Lecce[2], G. Mensitieri[3], E. Sacco[1] and M. Fraldi[1]

[1]Department of Structures for Engineering and Architecture, University of Napoli Federico II, Napoli, Italy
[2]NOVOTECH Aerospace Advanced Technology, Naples, Italy
[3]Department of Chemical, Materials and Production Engineering (DICMAPI), University of Napoli Federico II, Napoli, Italy
[4]Interdisciplinary Research Center for Structural Composites (SCIC), University of Napoli Federico II, Napoli, Italy

Abstract

The paper proposes a mixed strain- and stress-based topology optimization method for designing the ideal geometry of carbon fibers in composite laminates subjected to either applied tractions or prescribed displacements. On the basis of standard micromechanical approaches, analytical elastic solutions for a single cell, assumed to be a Representative Volume Element (RVE), are ad hoc constructed by involving anisotropy induced by fiber orientation and volume fraction, also taking into account inter-laminar stresses and strains. The analytical solutions are then implemented in a Finite Element (FE) custom-made topology optimization (TO) based procedure rewritten to have as output the best curves the reinforcing fibers have to draw in any composite laminate layer to maximize the overall panel stiffness or to minimize the elastic energy. To verify the effectiveness of the proposed strategy, different structures undergoing either in-plane or out-plane boundary conditions have been selected and theoretically investigated, determining the optimal fibers' maps and showing the related results in comparison to standard sequences of alternate fiber disposition for the same composites. Two optimized panels were at the end actually produced using an innovative Automated Fiber Placement (AFP) machine and consolidating the materials by means of autoclave curing processes, in this way replicating the fiber paths obtained from theoretical outcomes. As a control, two corresponding composite structures were also realized without employing the fiber optimization strategy. The panels have been tested in laboratory and the theoretical results have been compared with the experimental findings, showing a very good agreement with our predictions and confirming the capability of the proposed algorithm to suggest how to arrange the fibers to have enhanced mechanical performances. It is felt that the hybrid analytical-FE topology optimization strategy, in conjunction with the possibilities offered by AFP devices, could pave the way for a new generation of ultra-lightweight composites for aerospace, automotive and many industrial applications.

Keywords: Topology optimization, Automated Fiber Placement, composite structures, analytical solutions.

[1] Corresponding author: fraldi@unina.it

1. Introduction

Fiber Reinforced Composite structures have been widely applied in locomotive, aeronautical and aerospace engineering because of their high stiffness/weight ratios, driving on this topic more and more researchers in the last years.
The growing use of FRC in manufacturing has also gained an ever-increasing popularity in the optimal design of composite laminate shell structures, with the main goal of determining, for any desired performance, the proper choice of material and fiber orientation for each FRC layer (Foldager et al., 1998; Stegmann and Lund, 2005).
Optimal orientation of the fibers augments mechanical performance of the FRC with respect to the traditional quasi-isotropic fiber distribution and - at least in principle - with regards to any other standard laminate sequence (Wu, 2008; Tosh and Kelly, 2000; Gürdal and Olmedo 1993; Raju et al., 2012). In this framework, several optimization strategies have been proposed to enhance selected material properties of composites such as sizing, shape and topology optimization procedures, as a function of the different aspects of the structural design problem to be addressed. Among these techniques, Topology Optimization (TO) aims to determine the optimal distribution of the material within a prescribed design domain. Since the pioneering contribution by Bendsøe and Kikuchi (1988), TO has been mainly based on the maximization of the structural stiffness under total volume or mass constraints (Eschenauer and Olhoff, 2001; Bendsøe and Sigmund, 2003), that is minimizing the structural compliance. following this way, the material properties are interpolated by means of smooth functions of the design variable, i.e. the material density or an equivalent measure of the volume fraction, through the so-called SIMP (Solid Isotropic Material with Penalization) method, as proposed by Bendsøe (1989). However, if no porous or mass-depleted materials are object of optimization, the optimal design of structures can be also reached by assigning a specific material for the matrix, then fixing a reinforcement (i.e. short or long fibers) and thus identifying as design variable the fibers' volume fraction and/or their point-wise orientation, finally obtaining the percentage and/or the topology of the fibers to minimize elastic energy, by invoking the theory of homogenization for anisotropic materials.
In particular, for orthotropic materials, a general optimality criterion establishes that the structural compliance is minimized under given static and kinematic boundary conditions if stress and strain tensors locally share the same principal directions. This result was first obtained by Pedersen (1989) for bi-dimensional orthotropic solids, and later extended to three-dimensional orthotropic bodies by Rovati and Taliercio (2003). Three main gradient-driven approaches, corresponding to three different orthotropic material topology optimization strategies, were originally developed in order to determine the optimal layout of the structures: the so-called strain-based method (Cheng and Pedersen, 1997; Pedersen, 1990, 1989; Gea and Luo 2004), the stress-based method (Cheng and Kikuchi, 1994; Diaz and Bendsøe, 1992; Suzuki and Kikuchi, 1991) and the energy-based method (Luo and Gea, 1998). All the approaches mentioned above take into account the effect of the change in strain and stress due to the change in material orientation, searching the stiffest structure as that whose material symmetry planes allow to store the minimum amount of total elastic energy and, consequently, produce the minimum mean compliance. Moreover, all methods assume the invariance of strain and stress fields inside each design cell. The strain- and

stress-based methods provide that the optimality criterion be respectively expressed in the stress and in the strain form. On the other hand, the energy-based method requires that the dependency of strain and stress fields on material orientation be explored by introducing an energy factor in the inclusion model.

Alternative strategies still based on the gradient approach are material selection methods, such as Direct Material Optimization (DMO) (Sigmund and Torquato, 1997; Stegmann and Lund, 2005), Shape Function with Penalization (SFP) (Bruyneel, 2011) and Bi-value Coding Parameterization (BCP) (Gao et al., 2012). An evolution of curvilinear parameterization method has been also presented in the literature (Tatting and Gürdal, 2001; Wu 2008), consisting in the application of the Level Set method to optimization of fibers paths, by imposing a continuity of the fiber angles between elements (Brampton et al, 2015). In this case the solution is dependent on the initial configuration and the convergence is observed to be slow, requiring many iterations. In addition, the overall compliance of the level set solution results to be greater than that of the element solutions.

In this work, we *de facto* adapt the topology optimization to fiber-reinforced composites by prescribing the materials of both matrix and reinforcement and also constraining within technological (process-induced) ranges the volume fraction of fibers - a priori established by the ratio between the reinforcement and the matrix material in the tapes with which will be covered each selected lamina - in this manner searching elastic solutions at minimal energy over all possible families of curves that the continuous fibers can draw in any composite layer. To make this, an analytical solution is first proposed for a single orthotropic layer where the optimal orientation has been deduced minimizing the mean compliance of the structure subjected to prescribed either tractions or displacements. The effect of interlaminar stress and strains has been also taken into account with the aim of expanding the analytical solution for a single layer to the case of fiber-reinforced polymers with multiple layers. Therefore, the analytical procedure was implemented in a FE code to perform the optimization analyses.

Different examples have been selected in order to verify the effectiveness of the proposed strategy. A first structure - a rectangular panel alternatively subjected to either prescribed tractions or displacements inducing a main tensile regime - has been chosen with the aim of highlighting relevant and somehow complementary differences, in terms of fibers optimization maps, strictly related to the two *dual* applied boundary conditions. Further examples were therefore built up selecting structures experiencing either in-plane or out-of-plane boundary conditions for emphasizing the need of taking into account - or in other cases the possibility of neglecting - interlaminar stresses and strains. Finally, two optimized panels were at the end actually produced using an innovative Automated Fiber Placement (AFP) machine and by consolidating the materials by means of autoclave curing processes, so replicating the fiber paths obtained from theoretical outcomes. As a control, two corresponding composite structures were also realized without employing the fiber optimization strategy. The panels have been tested in laboratory and the theoretical results have been compared with the experimental findings, showing a very good agreement and confirming the effectiveness of the proposed strategy.

2. Methods

2.1. Problem formulation: analytical approach

Composite materials are used in the form of plates having two dimensions much greater than the third one. By following the approach proposed by Gea et al (2004) and by using the total potential energy functional Π, the weak formulation of linearly elastostatic problem for a two-dimensional structure, subjected to body force $\boldsymbol{f}$, surface tractions $\boldsymbol{t}$ along the boundary Γ_t and prescribed displacements $\boldsymbol{u}^0$ on Γ_d, can be written minimizing the functional

$$\min_{v}\Pi,\quad \Pi=\int_{\Omega}\frac{1}{2}C_{ijkl}\frac{\partial u_i}{\partial x_j}\frac{\partial v_k}{\partial x_l}d\Omega-\int_{\Omega}f_i v_i d\Omega-\int_{\Gamma_t}t_i v_i d\Gamma \tag{1}$$

where C_{ijkl} are the elastic moduli of the orthotropic material depending on both material properties and the orientation variable θ responsible of the local direction along which the reinforcing fiber is aligned, u_i represents the displacement satisfying this equation of motion and v_i stands for the virtual displacement that belongs to the kinematically admissible displacement set.

The stiffest structure is defined as the structure that stores the minimum amount of total internal elastic energy and, as consequence, has minimum mean compliance. We thus start by considering the elastic energy in correspondence of the solution Π and identify it as the objective function to be minimized, that is

$$2\Pi=\int_{\Omega}\sigma_{ij}\varepsilon_{ij}d\Omega=\int_{\Omega}C_{ijkl}\varepsilon_{ij}\varepsilon_{kl}d\Omega=\int_{\Omega}C_{ijkl}\frac{\partial u_i}{\partial x_j}\frac{\partial u_k}{\partial x_l}d\Omega$$

where σ_{ij} represent the stress components and ε_{ij} are the corresponding strains when the solution is found for any possible orientation variable θ.

Therefore, the optimality condition is obtained by making stationary the elastic energy with respect to the design variable, therefore imposing $\frac{\partial \Pi}{\partial \theta}=0$ so that

$$\frac{\partial \Pi}{\partial \theta}=\int_{\Omega}\left[\frac{\partial C_{ijkl}}{\partial \theta}\frac{\partial u_i}{\partial x_j}\frac{\partial u_k}{\partial x_l}+2C_{ijkl}\frac{\partial}{\partial \theta}\left(\frac{\partial u_i}{\partial x_j}\right)\frac{\partial u_k}{\partial x_l}\right]d\Omega \tag{2}$$

By recalling the principle of virtual displacements and deriving with respect to the orientation variable θ, then setting the virtual displacement v_k equal to u_k, one also obtains:

$$\int_{\Omega}\frac{\partial C_{ijkl}}{\partial \theta}\frac{\partial u_i}{\partial x_j}\frac{\partial u_k}{\partial x_l}d\Omega=-\int_{\Omega}C_{ijkl}\frac{\partial}{\partial \theta}\left(\frac{\partial u_i}{\partial x_j}\right)\frac{\partial u_k}{\partial x_l}d\Omega \tag{3}$$

By therefore combining the results (2) and (3), the optimality condition can be expressed as:

$$\frac{\partial \Pi}{\partial \theta} = -\int_{\Omega} \frac{\partial C_{ijkl}}{\partial \theta} \frac{\partial u_i}{\partial x_j} \frac{\partial u_k}{\partial x_l} d\Omega = 0$$

In terms of the finite element method, by discretizing the domain Ω in m elements, the optimality condition can be rewritten as:

$$\frac{\partial \Pi}{\partial \theta_e} = -\int_{\Omega^e} \frac{\partial C_{ijkl}}{\partial \theta_e} \frac{\partial u_i}{\partial x_j} \frac{\partial u_k}{\partial x_l} d\Omega^e = -\int_{\Omega^e} \frac{\partial C_{ijkl}}{\partial \theta_e} \varepsilon_{ij} \varepsilon_{kl} d\Omega^e = 0$$

where Ω^e represents the spatial extent of the e^{th} design cell. The strain and stress fields can be assumed as essentially uniform within each homogeneous design cell, if a sufficiently small size for the element is chosen. Then, by taking out of the integral the strain term in the above equation, the optimality condition in the strain form, i.e. in the cases of displacement-prescribed, can be expressed as:

$$\frac{\partial \Pi_\varepsilon}{\partial \theta_e} = -\boldsymbol{\varepsilon}_e^T \frac{\partial \mathbf{C}}{\partial \theta_e} \boldsymbol{\varepsilon}_e A_e = 0 \text{ with } e = 1, 2, .., m \tag{4}$$

where $\boldsymbol{\varepsilon}_e$ represents the strain vector, $\mathbf{C}$ is the rotated orthotropic stiffness matrix and A_e is the area of the e^{th} design cell, set as unity. Dually, the optimality condition in the stress form, i.e. in the cases of tractions-prescribed, can also be written as:

$$\frac{\partial \Pi_\sigma}{\partial \theta_e} = -\boldsymbol{\sigma}_e^T \frac{\partial \mathbf{S}}{\partial \theta_e} \boldsymbol{\sigma}_e = 0 \text{ with } e = 1, 2, .., m \tag{5}$$

where σ_e represents the stress vector and $\mathbf{S}$ is the rotated orthotropic compliance matrix (Pedersen and Pedersen, 2011; Klarbring and Stromberg, 2012).

In order to find the expression of the rotated stiffness and its inverse compliance matrix, that is $\bar{\mathbf{C}}$ and $\bar{\mathbf{S}}$ respectively, by essentially following the classical approach proposed by Barbero (1999, 2008), the in-plane linear stress-strain equations for the orthotropic design cell element can be written as

$$\begin{Bmatrix} \sigma_1 \\ \sigma_2 \\ \sigma_6 \end{Bmatrix}_e = \begin{bmatrix} \dfrac{E_1}{1-\upsilon_{12}\upsilon_{21}} & \dfrac{\upsilon_{12}E_2}{1-\upsilon_{12}\upsilon_{21}} & 0 \\ \dfrac{\upsilon_{12}E_2}{1-\upsilon_{12}\upsilon_{21}} & \dfrac{E_2}{1-\upsilon_{12}\upsilon_{21}} & 0 \\ 0 & 0 & G_{12} \end{bmatrix}_e \begin{Bmatrix} \varepsilon_1 \\ \varepsilon_2 \\ \gamma_6 \end{Bmatrix}_e$$

additionally considering the uncoupled equations for interlaminar shear stresses and strains, that is

$$\begin{Bmatrix} \sigma_4 \\ \sigma_5 \end{Bmatrix}_e = \begin{bmatrix} G_{23} & 0 \\ 0 & G_{13} \end{bmatrix}_e \begin{Bmatrix} \gamma_4 \\ \gamma_5 \end{Bmatrix}_e$$

where subscripts 1 and 2 denote respectively the fiber and the orthogonal-to-the-fiber directions, E_1 and E_2 are the orthotropic Young moduli, G_{12}, G_{23}, G_{13} are the shear moduli and υ_{12} is the Poisson's ratio in the plane referred to the subscripts.

Dually, the compliance equations for the orthotropic design cell element can be written as

$$\begin{Bmatrix} \varepsilon_1 \\ \varepsilon_2 \\ \gamma_6 \end{Bmatrix}_e = \begin{bmatrix} \frac{1}{E_1} & -\frac{\upsilon_{12}}{E_1} & 0 \\ -\frac{\upsilon_{12}}{E_1} & \frac{1}{E_2} & 0 \\ 0 & 0 & \frac{1}{G_{12}} \end{bmatrix}_e \begin{Bmatrix} \sigma_1 \\ \sigma_2 \\ \sigma_6 \end{Bmatrix}_e$$

by additionally considering the uncoupled equations for interlaminar shear stresses and strains, that is

$$\begin{Bmatrix} \gamma_4 \\ \gamma_5 \end{Bmatrix}_e = \begin{bmatrix} \frac{1}{G_{23}} & 0 \\ 0 & \frac{1}{G_{13}} \end{bmatrix}_e \begin{Bmatrix} \sigma_4 \\ \sigma_5 \end{Bmatrix}_e$$

Transforming stresses, strains, compliance and stiffness by means of the following rotation matrix $\boldsymbol{T}$

$$[\boldsymbol{T}] = \begin{bmatrix} \cos^2\theta & \sin^2\theta & 2\cos\theta\sin\theta \\ \sin^2\theta & \cos^2\theta & -2\cos\theta\sin\theta \\ -\cos\theta\sin\theta & \cos\theta\sin\theta & \cos^2\theta - \sin^2\theta \end{bmatrix}$$

so that

$$\overline{\mathbf{C}} = \boldsymbol{T}^{-1}\mathbf{C}\boldsymbol{T}^{-T} \text{ and } \overline{\mathbf{S}} = \boldsymbol{T}^{-1}\mathbf{S}\boldsymbol{T}^{-T}$$

from material coordinate system (1,2,3) to the rotated by the angle θ global coordinate system (x,y,z), the components of the rotated reduced and interlaminar stiffness matrix, $\overline{E}_{ij}$, can be obtained for the orthotropic design cell element as

$$\bar{E}_{11} = E_{11}\cos^4\theta + 2(E_{12} + 2E_{66})\sin^2\theta\cos^2\theta + E_{22}\sin^4\theta$$
$$\bar{E}_{12} = (E_{11} + E_{22} - 4E_{66})\sin^2\theta\cos^2\theta + E_{12}(\sin^4\theta + \cos^4\theta)$$
$$\bar{E}_{22} = E_{11}\sin^4\theta + 2(E_{12} + 2E_{66})\sin^2\theta\cos^2\theta + E_{22}\cos^4\theta$$
$$\bar{E}_{16} = (E_{11} - E_{12} - 2E_{66})\sin\theta\cos^3\theta + (E_{12} - E_{22} + 2E_{66})\sin^3\theta\cos\theta$$
$$\bar{E}_{26} = (E_{11} - E_{12} - 2E_{66})\sin^3\theta\cos\theta + (E_{12} - E_{22} + 2E_{66})\sin\theta\cos^3\theta$$
$$\bar{E}_{66} = (E_{11} + E_{22} - 2E_{12} - 2E_{66})\sin^2\theta\cos^2\theta + E_{66}(\sin^4\theta + \cos^4\theta)$$
$$\bar{E}_{44} = E_{44}\cos^2\theta + E_{55}\sin^2\theta$$
$$\bar{E}_{55} = E_{44}\sin^2\theta + E_{55}\cos^2\theta$$
$$\bar{E}_{45} = (E_{55} - E_{44})\sin\theta\cos\theta$$

where $E_{11} = \dfrac{E_1}{1-\nu_{12}\nu_{12}}$, $E_{12} = \dfrac{\nu_{12}E_1}{1-\nu_{12}\nu_{12}}$ $E_{22} = \dfrac{E_2}{1-\nu_{12}\nu_{12}}$, $E_{66} = G_{12}$, $E_{44} = G_{23}$, $E_{55} = G_{13}$.

Similarly, the components of the rotated compliance matrix, $\bar{S}_{ij}$, can be written as follows

$$\bar{S}_{11} = S_{11}\cos^4\theta + 2(S_{12} + S_{66})\sin^2\theta\cos^2\theta + S_{22}\sin^4\theta$$
$$\bar{S}_{12} = (S_{11} + S_{22} - S_{66})\sin^2\theta\cos^2\theta + S_{12}(\sin^4\theta + \cos^4\theta)$$
$$\bar{S}_{22} = S_{11}\sin^4\theta + (2S_{12} + 2S_{66})\sin^2\theta\cos^2\theta + S_{22}\cos^4\theta$$
$$\bar{S}_{16} = (2S_{11} - 2S_{12} - S_{66})\sin\theta\cos^3\theta - (2S_{22} - 2S_{12} - S_{66})\sin^3\theta\cos\theta$$
$$\bar{S}_{26} = (2S_{11} - 2S_{12} - S_{66})\sin^3\theta\cos\theta - (2S_{22} - 2S_{12} - S_{66})\sin\theta\cos^3\theta$$
$$\bar{S}_{66} = 2(2S_{11} + 2S_{22} - 4S_{12} - S_{66})\sin^2\theta\cos^2\theta + S_{66}(\sin^4\theta + \cos^4\theta)$$
$$\bar{S}_{44} = S_{44}\cos^2\theta + S_{55}\sin^2\theta$$
$$\bar{S}_{55} = S_{44}\sin^2\theta + S_{55}\cos^2\theta$$
$$\bar{S}_{44} = (S_{55} - S_{44})\sin\theta\cos\theta$$

where $S_{11} = \dfrac{1}{E_1}$, $S_{12} = \dfrac{-\nu_{12}}{E_1}$, $S_{22} = \dfrac{1}{E_2}$, $S_{66} = \dfrac{1}{G_{12}}$, $S_{44} = \dfrac{1}{G_{23}}$ and $S_{55} = \dfrac{1}{G_{13}}$.

Algebraic manipulations allow to rewrite the optimality conditions (4) and (5) in the displacement-prescribed case as follows

$$\begin{aligned}
\frac{\partial \Pi_\varepsilon}{\partial \theta_e} &= \frac{1}{2}[(E_{11} - E_{22})\gamma_{xy}(\epsilon_x + \epsilon_y) + 2(-E_{44} + E_{55})\gamma_{xz}\gamma_{yz}]\cos 2\theta_e + \\
&+ \frac{1}{2}(E_{11} - 2E_{12} + E_{22} - 4E_{66})\gamma_{xy}(\epsilon_x - \epsilon_y)\cos 4\theta_e \\
&- \frac{1}{2}[(E_{11} - E_{22})(\epsilon_x - \epsilon_y)(\epsilon_x + \epsilon_y) - (E_{44} - E_{55})(\gamma_{xz} - \gamma_{yz})(\gamma_{xz} + \gamma_{yz})]\sin 2\theta_e \\
&- \frac{1}{4}(E_{11} - 2E_{12} + E_{22} - 4E_{66})(\epsilon_x - \gamma_{xy} - \epsilon_y)(\epsilon_x + \gamma_{xy} - \epsilon_y)\sin 4\theta_e
\end{aligned}$$

and, in the cases of tractions-prescribed, as

$$
\begin{aligned}
\frac{\partial \Pi_\sigma}{\partial \theta_e} &= [(S_{11}-S_{22})\tau_{xy}(\sigma_x+\sigma_y)+(-S_{44}+S_{55})\tau_{xz}\tau_{yz}]\cos 2\theta_e \\
&+(S_{11}-2S_{12}+S_{22}-S_{66})\tau_{xy}(\sigma_x-\sigma_y)\cos 4\theta_e \\
&-\frac{1}{2}[(S_{11}-S_{22})(\sigma_x-\sigma_y)(\sigma_x+\sigma_y)-(S_{44}-S_{55})(\tau_{xz}-\tau_{yz})(\tau_{xz}+\tau_{yz})]\sin 2\theta_e \\
&-\frac{1}{4}(S_{11}-2S_{12}+S_{22}-S_{66})[-4\tau_{xy}^2+(\sigma_x-\sigma_y)^2]\sin 4\theta_e
\end{aligned}
$$

where both strain and stress components refer to values at the centroid of the design cell. By setting the above equations to zero, both expressions can be arranged in the following form

$$a\cos 2\theta_e + b\cos 4\theta_e + c\cos 2\theta_e + d\sin 4\theta_e = 0 \tag{6}$$

where, in case of prescribed displacements it is

$$
\begin{aligned}
a &= \frac{1}{2}[(E_{11}-E_{22})\epsilon_{xy}(\epsilon_x+\epsilon_y)+2(-E_{44}+E_{55})\epsilon_{xz}\epsilon_{yz}] \\
b &= \frac{1}{2}(E_{11}-2E_{12}+E_{22}-4E_{66})\epsilon_{xy}(\epsilon_x-\epsilon_y) \\
c &= \frac{1}{2}[-(E_{11}-E_{22})(\epsilon_x-\epsilon_y)(\epsilon_x+\epsilon_y)+(E_{44}-E_{55})(\epsilon_{xz}-\epsilon_{yz})(\epsilon_{xz}+\epsilon_{yz})] \\
d &= -\frac{1}{4}(E_{11}-2E_{12}+E_{22}-4E_{66})(\epsilon_x-\epsilon_{xy}-\epsilon_y)(\epsilon_x+\epsilon_{xy}-\epsilon_y)
\end{aligned}
$$

while, for prescribed tractions, one has

$$
\begin{aligned}
a &= (S_{11}-S_{22})\sigma_{xy}(\sigma_x+\sigma_y)+(-S_{44}+S_{55})\sigma_{xz}\sigma_{yz} \\
b &= (S_{11}-2S_{12}+S_{22}-S_{66})\sigma_{xy}(\sigma_x-\sigma_y) \\
c &= \frac{1}{2}[-(S_{11}-S_{22})(\sigma_x-\sigma_y)(\sigma_x+\sigma_y)+(S_{44}-S_{55})(\sigma_{xz}-\sigma_{yz})(\sigma_{xz}+\sigma_{yz})] \\
d &= -\frac{1}{4}(S_{11}-2S_{12}+S_{22}-S_{66})[-4\sigma_{xy}^2+(\sigma_x-\sigma_y)^2]
\end{aligned}
$$

It is worth noticing that the above listed coefficients depend both on stiffness and compliance moduli and on the states of plane stress and strain as well, including interlaminar shear stresses and strains.
By setting $x = 2\theta_e$, the previous equation (6) can be rearranged in the following form

$$a\cos x + b\cos 2x + c\sin x + d\sin 2x = 0 \tag{7}$$

Moreover, by making the substitutions

$$t = tg\,\frac{x}{2}, \sin x = \frac{2t}{1+t^2}, \cos x = \frac{1-t^2}{1+t^2}, \sin 2x = \sin x \cos x = \frac{2t(1-t^2)}{(1+t^2)^2}, \cos 2x = \frac{2(1-t^2)^2}{(1+t^2)^2}$$

the equation (7) can be finally expressed as

$$c_1 t^4 + c_2 t^3 + c_3 t^2 + c_4 t + c_5 = 0 \tag{8}$$

where $c_1 = -a + b$, $c_2 = 2c - 4d$, $c_3 = -6b$, $c_4 = 2c + 4d$ and $c_5 = a + b$.
The fourth-order polynomial equation (8) can be analytically solved by means of the general Ferrari-Cardano formula (*Ars Magna*, 1545). Then, for each value t_i, the corresponding value of the angle θ_{e_i} can be obtained by means of

$$\theta_{e_i} = \mathrm{arctg}\, t_i$$

Finally, for each real value of the angle θ_{e_i}, one can easily compute the corresponding value of the strain energy, the optimal angle value, θ_{OPT}, being finally chosen equal to that corresponding to the minimum value of the strain energy.

2.2. Sensitivity analyses

With the aim of highlighting the qualitative behaviors of the optimal solutions obtained for a single cell in both the case of displacement and tractions prescribed, the Young modulus along the fiber direction has been set to unit and the Young modulus orthogonal to the fibers has been set to 0.05, assuming a standard value of 0.3 for the Poisson's ratio.
In the Fig. 1 are collected the theoretical optimal conditions in which the stucture is subjected to both prescribed-displacements than prescribed-tractions, and the results are evaluated by fixing the strains $\varepsilon_x, \varepsilon_{xy}, \varepsilon_y$ and the stresses $\sigma_x, \sigma_{xy}, \sigma_y$ opportunely equal to 0 and 1 (in both cases the interlaminar contributions of the strain and stress are neglecting).

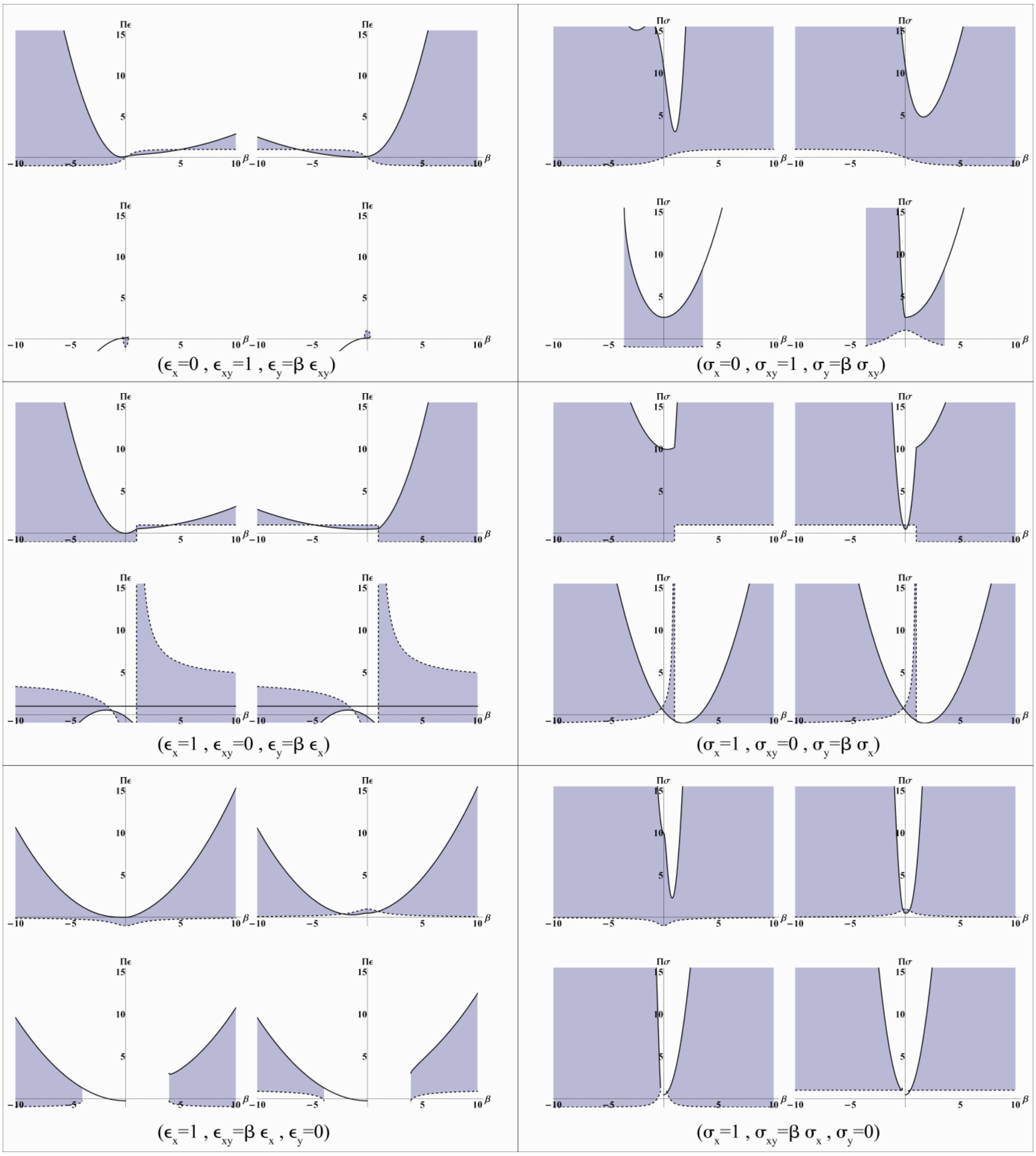

Fig. 1: Energies plot by setting $\varepsilon_x = 0$, $\varepsilon_{xy} = 1$, $\varepsilon_y = \beta\varepsilon_{xy}$ and varying β in the range [-10,10] (upper left: 1th value of θ_{OPT}, upper right: 2nd value of θ_{OPT}, lower left: 3rd value of θ_{OPT}, lower right: 4th value of θ_{OPT}).

Moreover, reducing the range of β where the corresponding θ_{OPT} have sense and constructing related energies as piecewise functions of β, the following graphs (Fig. 2) plot the profile of the energy minima over β, in the case of prescribed-displacements and prescribed-tractions in the same cases studied previously.

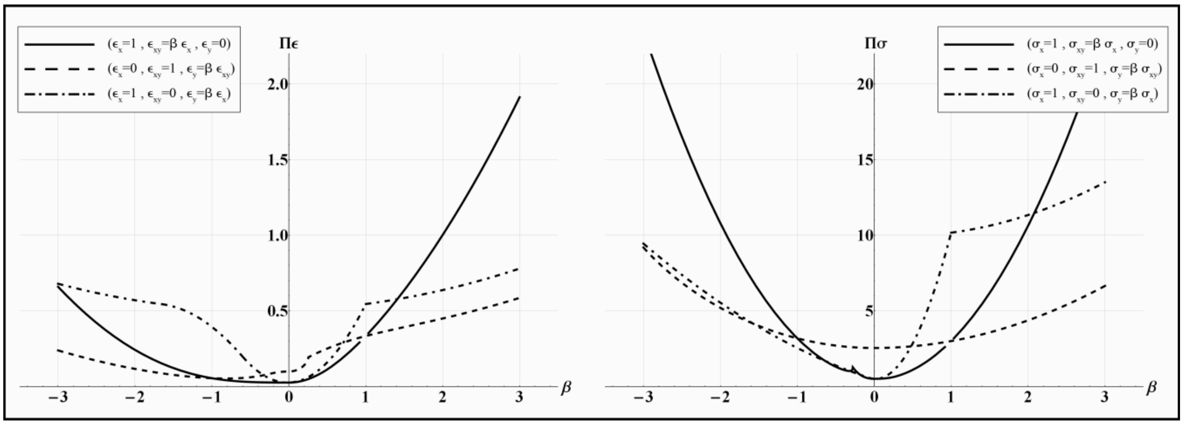

Fig. 2: By setting $\sigma_x = 0$, $\sigma_{xy} = 1$, $\sigma_y = \beta\sigma_{xy}$, plot of the energy minima over β.

3. Results

3.1. FE-based numerical approach

Finite element analyses have been performed covering the analytical approach above explained by means of a custom-made procedure developed by APDL (Ansys Parametric Design Language) in Ansys10® Multiphysics environment (Ansys Inc., Canonsburg, PA, USA). With the aim of obtaining the solution of the quartic equation (8), with the substantial advantage of avoiding to manage imaginary roots, an external call to Mathematica® (Wolfram, Champaign, IL, USA) has been run at the end of each numerical analysis, exchanging data from Ansys® to Mathematica® and vice versa by means of a text file. That is, at the end of each numerical iteration, the coefficients of the quartic equation (8), calculated by Ansys, have been written on disk; using the Mathematica® native language, a package has been written in order to read data from disk, to solve the quartic equation (8) for each element of the structure and to give back the obtained results to Ansys. Then, the potential optimal angles have been tested calculating the strain energy for each element of the structure; hence, the procedure selects as optimal angle that one corresponding to the lower value of the strain energy of the design cell. Thus, the two optimal angle maps, produced via both strain- and stress-based methods, were compared with reference to the strain energy of the whole examined structure; in other words, the procedure loads the angles map corresponding to the lower value of the strain energy of the structure, ending to iterate when the strain energies perceptual difference of two consecutive steps becomes less than the input energy tolerance.

At the end of the optimization process, in order to measure the vantage obtained by the optimization procedure, the quantity Strain Energy Gain (SEG), defined as the Strain Energy perceptual difference of the structure before and after optimization, has been calculated

$$SEG = \frac{SE_{PRE-OPT} - SE_{OPT}}{SE_{OPT}}$$

Flow chart of the main part of the adopted numeric procedure is showed in the Fig. 3.

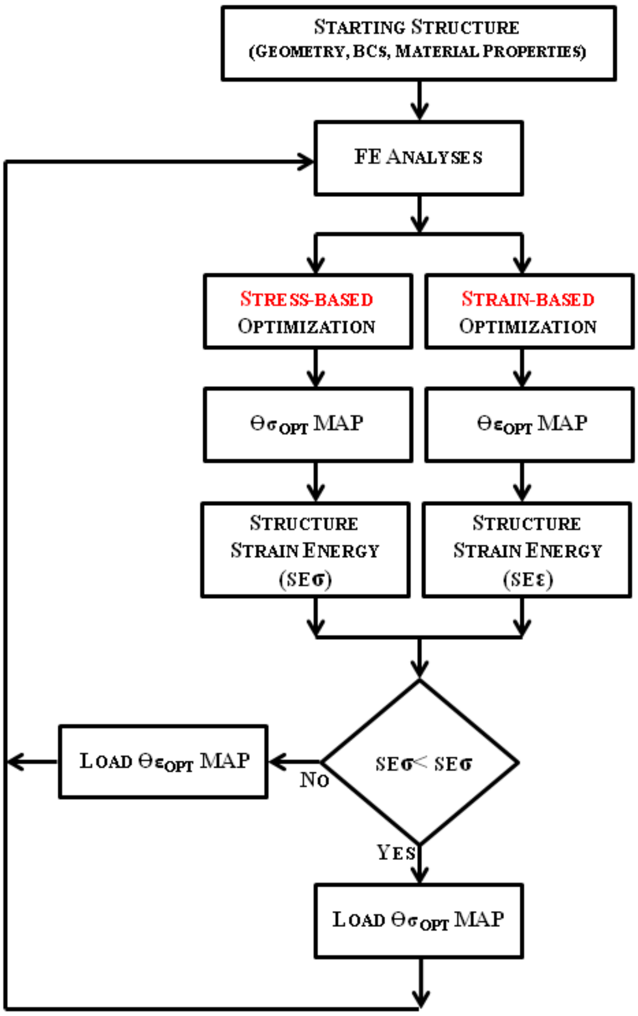

Fig. 3: Flow chart of the main part of the adopted numeric procedure

3.2. Example applications

In order to verify the effectiveness of the proposed strategy, different structures (i.e. FRC panels), subject to either applied tractions or prescribed displacements and either to in- or out-plane boundary conditions, have been selected and analyzed by means of the FE-based procedure. The material has been set as 8 layers composite (Thermoplastic Composite APC-2/AS4 with $E_1 = 138$ MPa, $E_2 = E_3 = 10$ MPa, $G_{12} = G_{13} = 5.65$ MPa, $G_{23} = 3.7$ MPa, $\upsilon_{12} = \upsilon_{13} = .28$ and $\upsilon_{23} = .33$) with different orientations for each layer ($\theta_1 = 0$, $\theta_2 = 90$, $\theta_3 = 45$, $\theta_4 = -45$, $\theta_5 = -45$, $\theta_6 = 45$, $\theta_7 = 90$ and $\theta_8 = 0$), so that a quasi-isotropic behavior can be assumed. Element type has been set as hexahedral multi-layer solid-shell with eight nodes (three degrees of freedom for each node and linear shape functions), sizing the height of the element equal to the panels thickness. Moreover, structures have been meshed dense enough so that strains and the stress fields can be reasonably assumed constant inside each element.

3.2.1. *In-plane boundary conditions example: rectangular panel in tension regime*

The first example is paradigmatic: a rectangular panel (L=1000 mm, H=500 mm, thickness=2.24 mm) in classical tensile regime, that is, the minor sides of the structure subject to either tractions (F=1 N) or displacements (δ=10 mm) along the major direction of the structure.

Boundary conditions applied on the meshed structure are showed in the Fig. 4 in the case of prescribed tractions (left) and prescribed displacements (right)

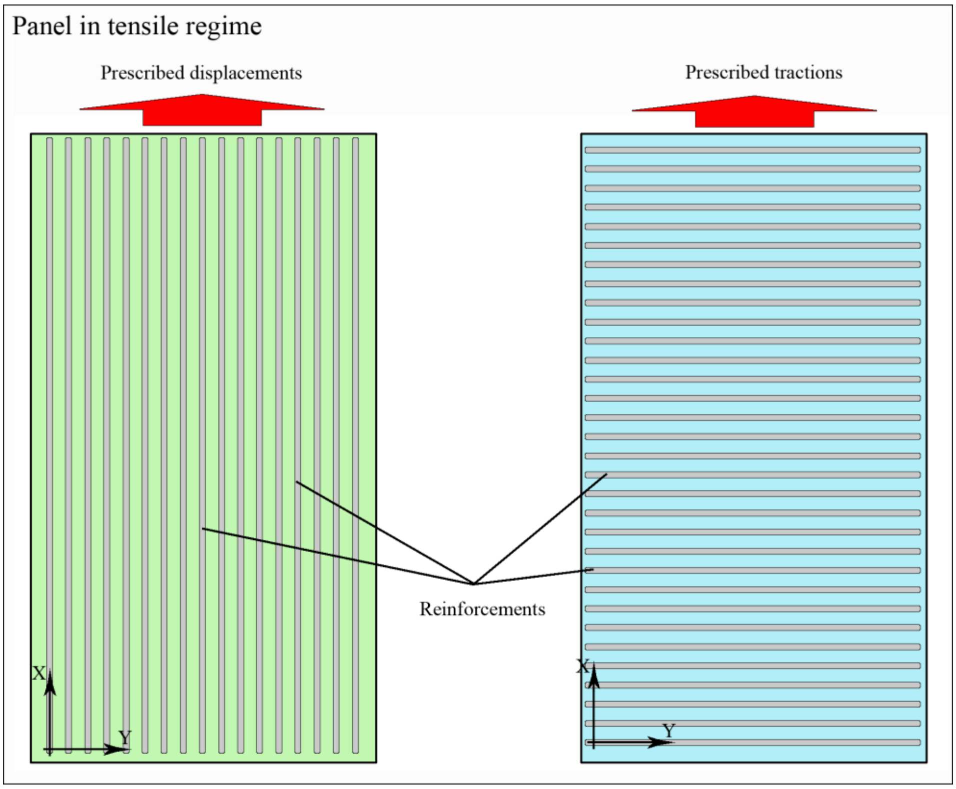

Fig. 4 Geometry, BCs and optimized fiber orientation maps for rectangular panels in tensile regime in the case of (left) prescribed displacements and (right) prescribed tractions.

By observing the obtained optimal fibers orientation maps, it is worth to highlight the dual behavior of the structure. As expected, when the structure is subject to prescribed tractions, the optimal configuration furnish fibers oriented along the major direction of the structure, as well as along the direction of the loading, in this way maximizing the structural stiffness of the system. Dually, when the structure is subject to prescribed displacements, the optimal configuration provides fibers oriented along the minor direction of the structure, as well as orthogonal to the direction of the loading, in this way maximizing the structural compliance, i.e. minimizing the structural stiffness of the system. For all the examined cases, the optimization strategy furnish the same fibers disposition for each layer.

3.2.2. *In-plane boundary conditions example: cantilever panel*

Next example is a rectangular panel (L=500 mm, H=200 mm, thickness=2.24 mm) in the classical cantilever configuration, that is, one minor side of the structure fully constrained and the opposite side subject to traction (F=1000 N) in the plane of the structure. A scheme of the examined structure is showed in the Fig. 5a and the optimal fibers orientation map for the first layer is showed in the Fig. 5b. Moreover, displacements along y-axis (up) and Von Mises stress developed in the panel are collected in the case of quasi-isotropic (c and e) and optimized (d and f) structure, by regarding to interlaminar stresses and strains.

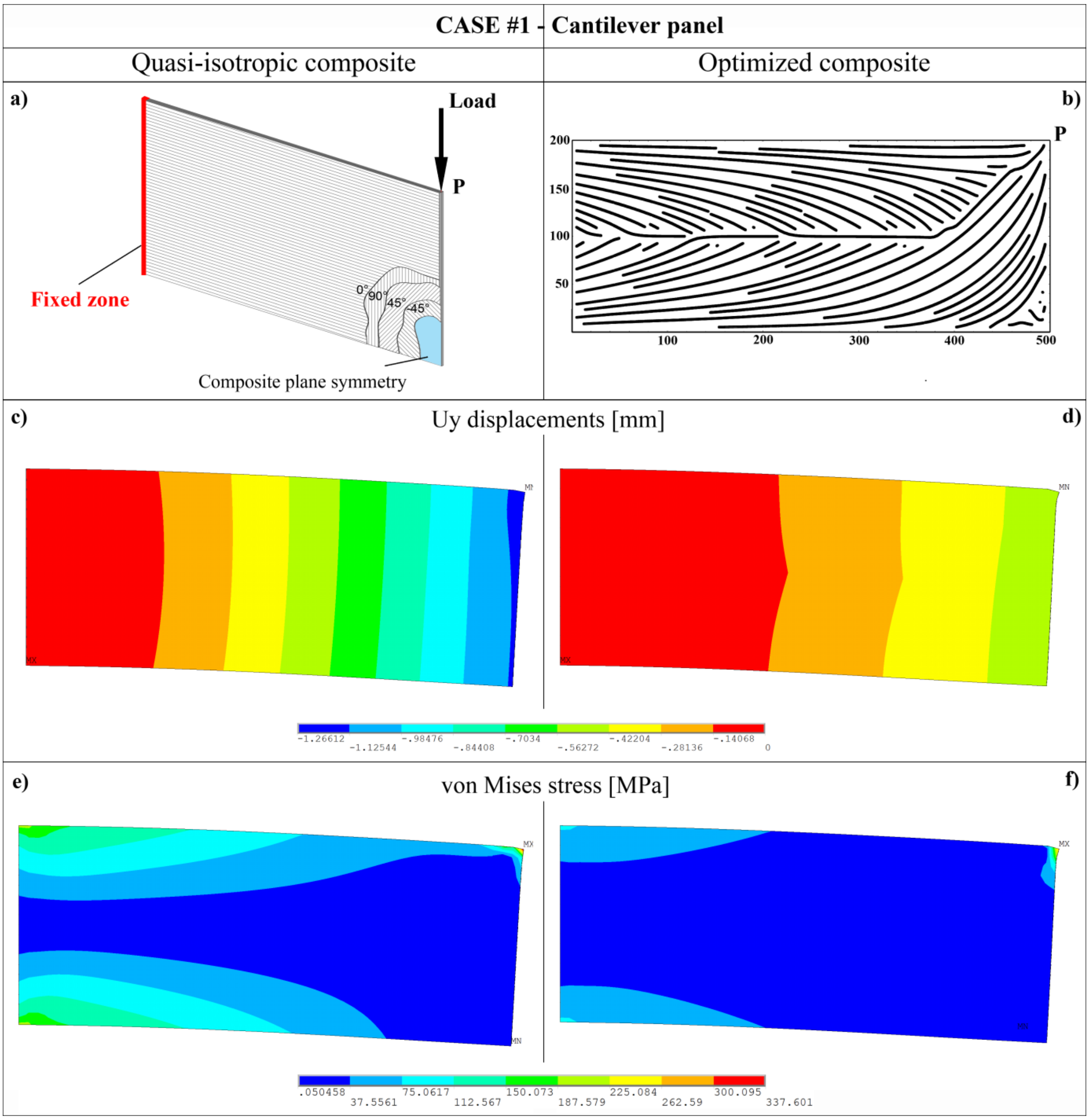

Fig. 5: a) Geometry and BCs for rectangular panel in cantilever configuration; b) optimal fibers orientation maps, by regarding to interlaminar stresses and strains. Displacements along y-axis and Von Mises stress contour plot of the first layer of the panel in the case of no optimized (c and e) and optimized structure (d and f).

When neglecting interlaminar stresses and strains, the structure exhibits no difference in terms of fibers maps, displacements along z-axis and Von Mises stress, respect to the case when interlaminar stresses and strains are considered. Moreover, it is significantly to be noted the arrangement of the fibers, with a ±45 degrees disposition near the clamped side and directed to the corner where the load is applied.

3.2.3. *Out-Plane boundary conditions example: square panels in bending regime*

The first example in bending regime is a square panel (L=500 mm, H=500 mm, thickness=2.24 mm), where two adjacent sides of the structure have been fully constrained and the opposite corner subjected to traction (F=10 N) orthogonal to the panel, along z-axis. A scheme of the examined structure and the optimal fibers orientation map for the first layer are showed in the Fig. 6a and 6b, respectively. In addition, displacements along y-axis (up) and Von Mises stress are collected in the Fig.6, in the case of quasi-isotropic (c and e) and optimized (d and f) structure, by regarding to interlaminar stresses and strains.

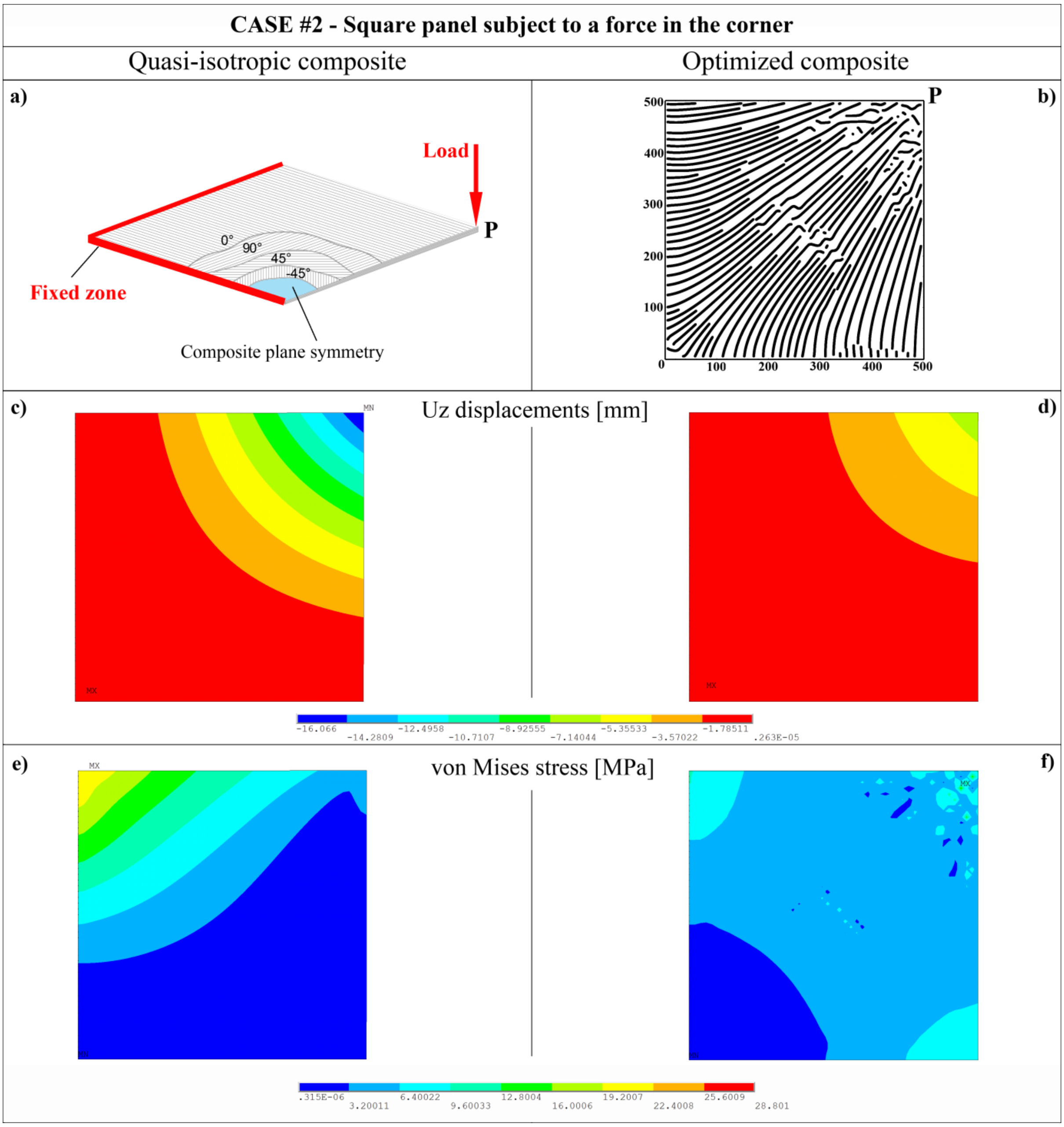

Fig. 6: a) Geometry and BCs for square panel in bending regime; b) optimal fibers orientation maps, by regarding to interlaminar stresses and strains. Displacements along y-axis (a) and Von Mises stress (e) contour plot of the first layer of the panel in the case of no optimized (c and e) and optimized structure (d-f).

By regarding to interlaminar stresses and strains, the structure exhibits a lower displacement along z-axis with a perceptual difference equal to 1.04% respect to the case when interlaminar stresses and strains are neglected. It is to be noted that the fibers start orthogonal to the clamped side and results directed to the corner where the load is applied.

Next example in bending regime is a square panel (L=500 mm, H=500 mm, thickness=2.24 mm), where all sides of the structure have been fully constrained and the center of the panel subjected to orthogonal to the panel traction (F=10 N). A scheme of the examined structure and the optimal fibers orientation map for the first layer are showed in the Fig. 7a and 7b, respectively. In addition, displacements along y-axis (up) and Von Mises stress are collected in the Fig. 7, in the case of quasi-isotropic composite (c and e) and optimized (d and f) structure, by regarding to interlaminar stresses and strains.

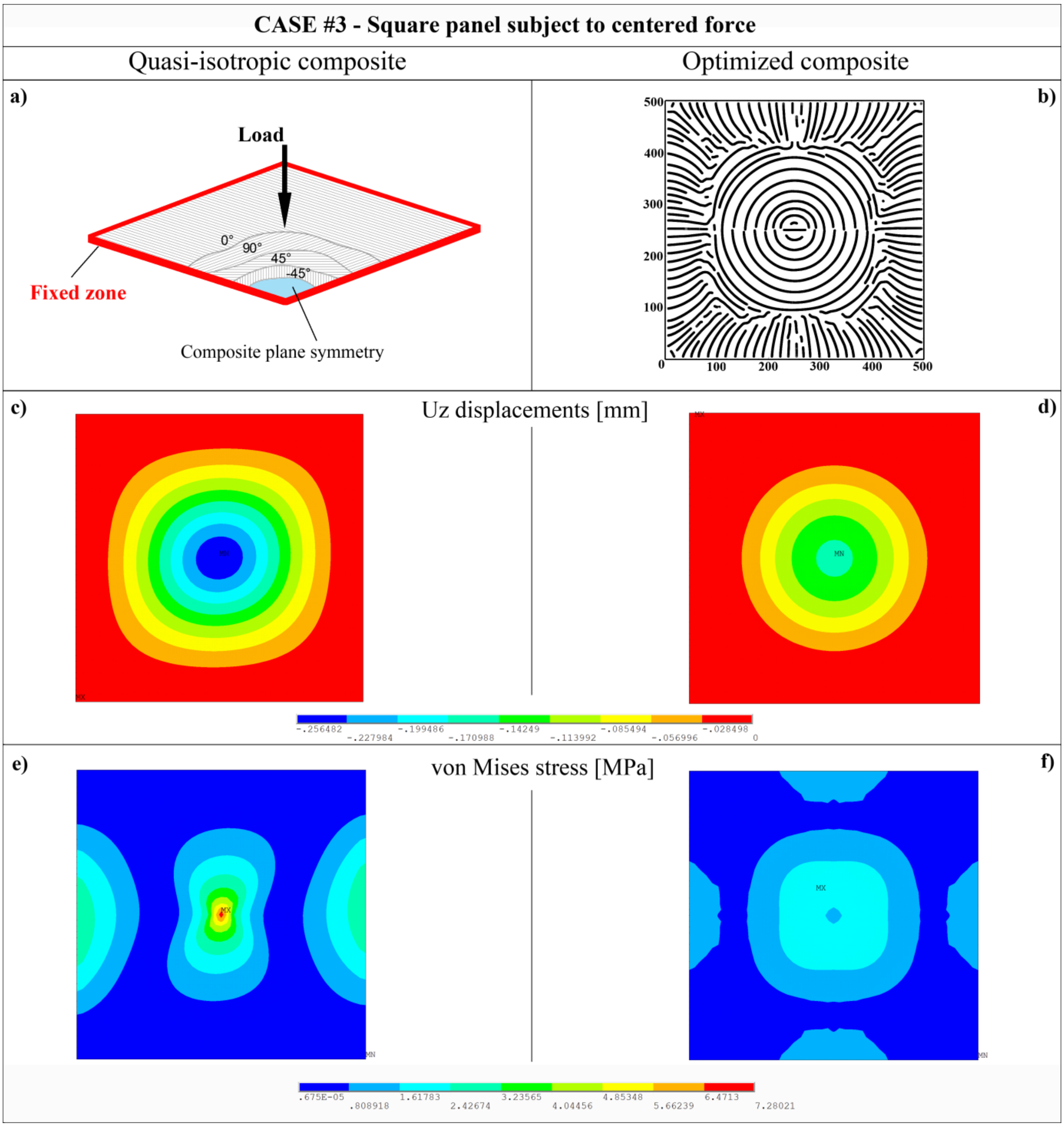

Fig.7: a) Geometry and BCs for square panel in bending regime; b) optimal fibers orientation maps, by regarding to interlaminar stresses and strains Displacements along y-axis (a) and Von Mises stress (e) contour plot of the first layer of the panel in the case of no optimized (c and e) and optimized structure (d-f).

By regarding to interlaminar stresses and strains, the structure exhibits a lower displacement along z-axis with a perceptual difference equal to 0.16% respect to the case when interlaminar stresses and strains are neglected. It is to be noted the arrangement of the fibers, starting orthogonal to the clamped side and disposing in circle around the point where the load is applied.

The last example in bending regime is a square panel (L=500 mm, H=500 mm, thickness=2.24 mm), where all corners of the structure have been fully constrained and moments (2.24 Nmm) applied on all sides of the panel, as the scheme showed in the Fig.8a. Numerical results in terms of displacements and von Mises stresses are shown in the Fig. 8, in the case of quasi-isotropic (c and e) and optimized (d and f) structure, by regarding to interlaminar stresses and strains.

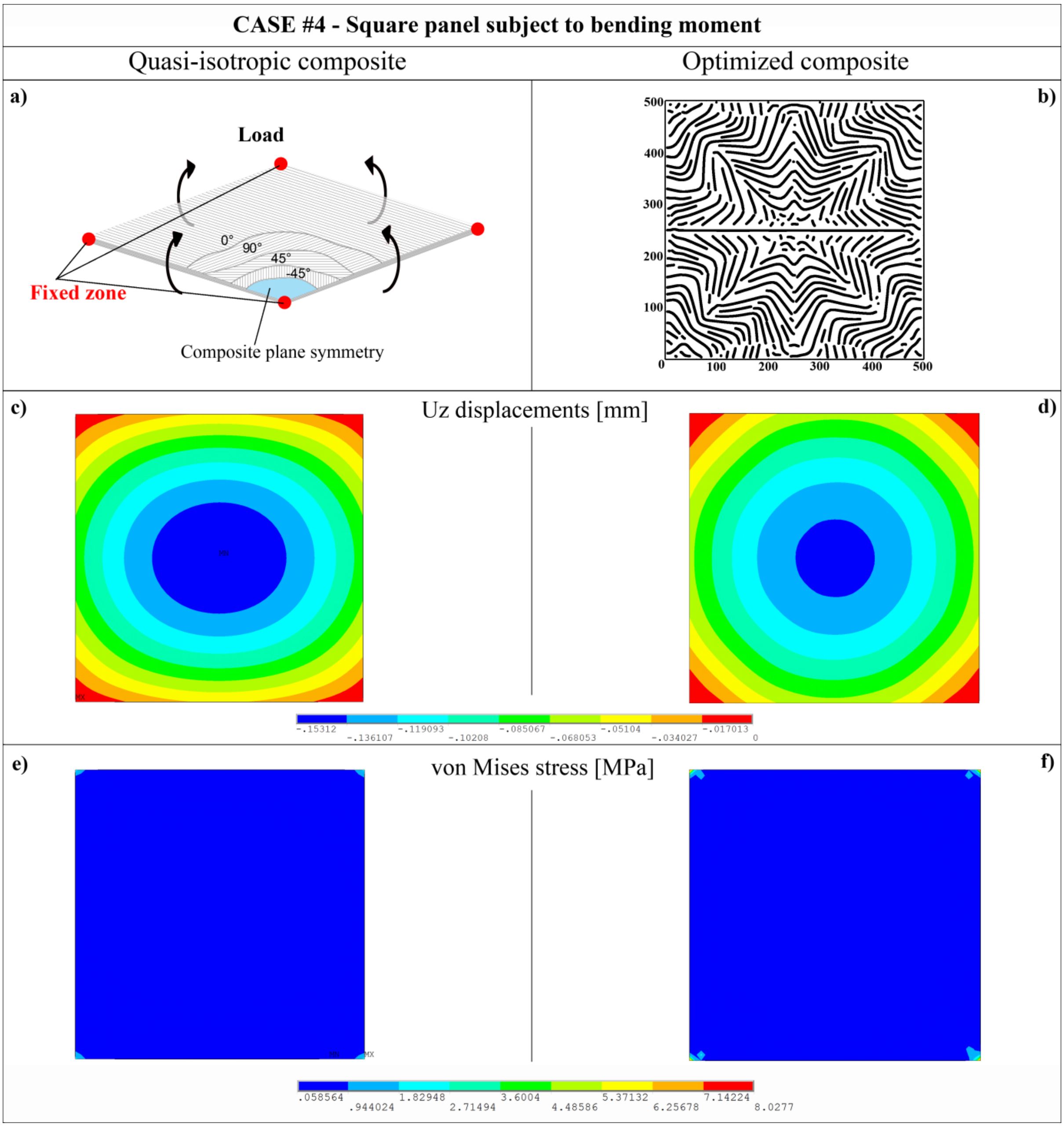

Fig.8: a) Geometry and BCs for square panel in bending regime; b) optimal fibers orientation maps, by regarding to interlaminar stresses and strains. Displacements along y-axis (a) and Von Mises stress (e) contour plot of the first layer of the panel in the case of no optimized (c and e) and optimized structure (d-f).

In this case, the structure exhibits a lower displacement along z-axis with a perceptual difference equal to 0.64%, respect to the case when interlaminar stresses and strains are neglected. Optimized fibers disposition, shown in Fig. 8b, appears symmetric and regular, arranging the fibers in a flower style.

3.2.4. *Out-Plane boundary conditions example: torsion regime*

Next example is a rectangular panel (L=500 mm, H=200 mm, thickness=2.24 mm) fully constrained at the center of minor sides and subjected to torsion (3.33E-03 Nmm). The boundary conditions are showed in the Fig.9 a. Displacements along y-axis (up) and Von Mises stress are collected in the Fig. 9, in the case of quasi-isotropic (c and e) and optimized (d and f) structure, by regarding to interlaminar stresses and strains.

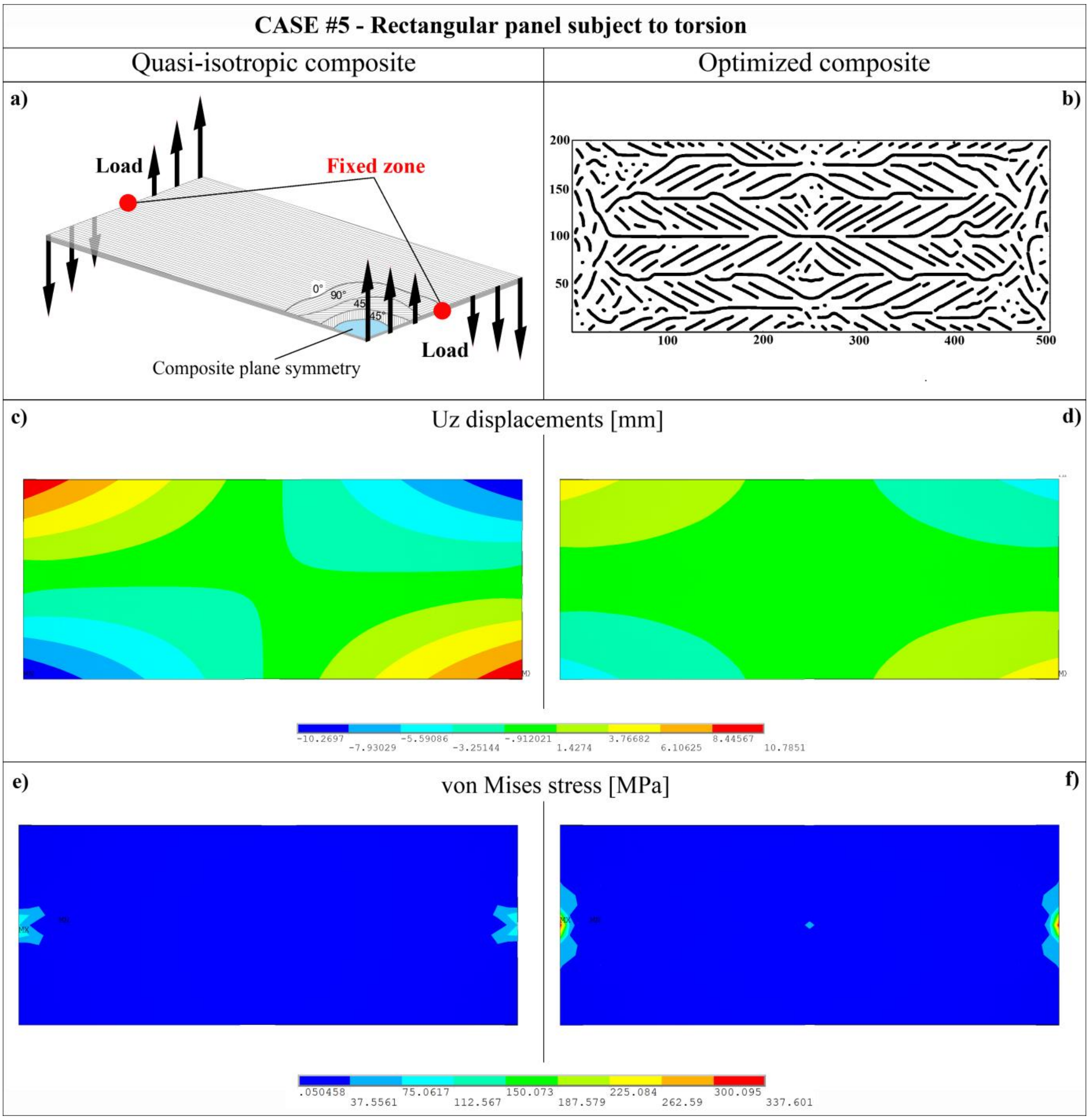

Fig. 9: Geometry and BCs for rectangular panel in torsion regime; b) optimal fibers orientation maps by regarding to interlaminar stresses and strains. Displacements along y-axis (a) and Von Mises stress (e) contour plot of the first layer of the panel in the case of no optimized (c and e) and optimized structure (d-f).

By regarding to interlaminar stresses and strains, the structure exhibits a greater displacement along z-axis with a perceptual difference equal to 0.81% respect to the case when interlaminar stresses and strains are neglected. This structure has been also analyzed when subjected to rotation (φ=0.001), showing similarity in the both displacements and stress fields. The comparison between the arrangements of the fibers is shown in the Fig.10, in the case of prescribed rotations (a) and prescribed torsion (b). When the structure is subject to torsion, the fibers are substantially arranged with a ± 45 degrees disposition. When the structure is subject to rotation, the fibers start orthogonal to the sides, arranging with a not preferred orientation in the center of the panel.

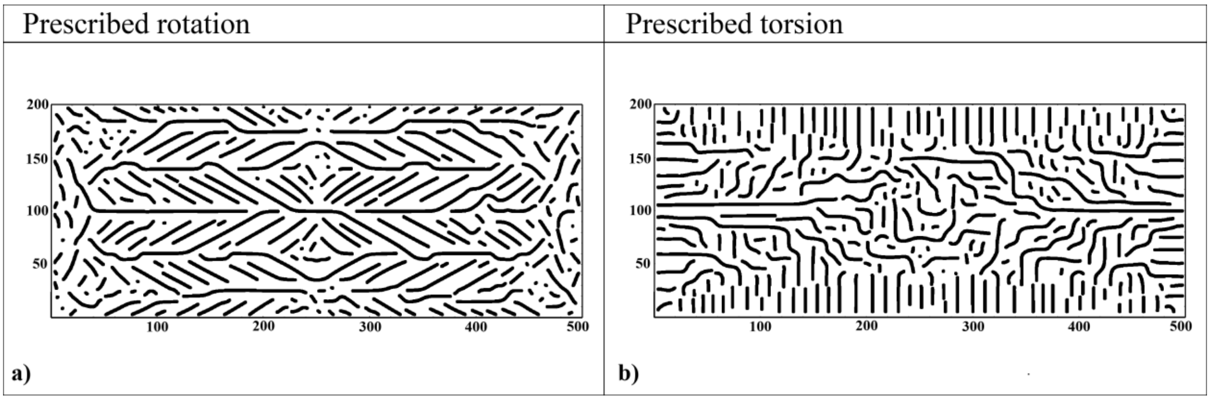

Fig. 10: Comparison between the reinforcement arrangements obtained in the case of panel under torsion regime, in the case of prescribed rotations (a) and prescribed torsion (b).

3.3. Experimental results

3.3.1. *Manufacturing*

The fiber steering capabilities of the AFP machine has been used to investigate design flexibility and limitations of the AFP process for the development of more efficient composite structures. The AFP plates were laid up using the Coriolis Composites fiber placement machine installed at Novotech Aerospace Advanced Technology s.r.l., Italy (see Fig. 11).

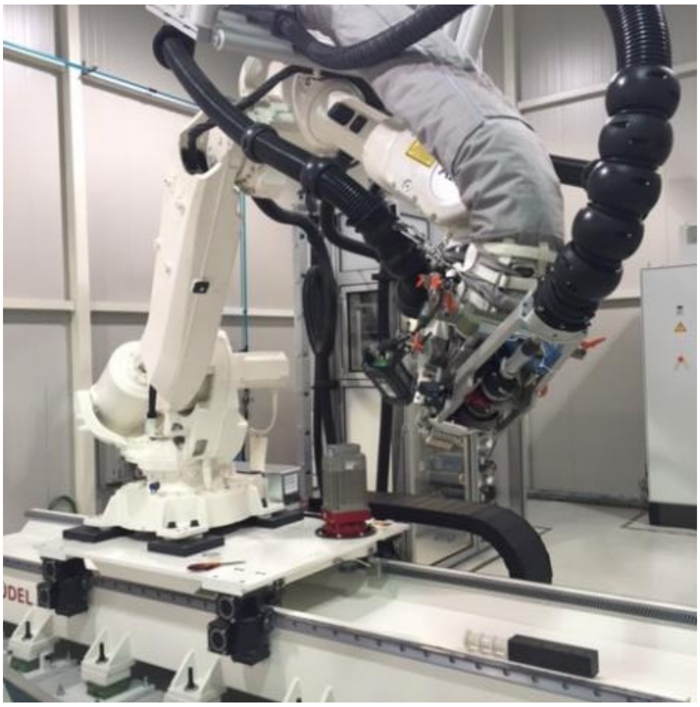

Fig. 11 - Coriolis AFPM at Novotech plant.

This machine is composed of an ABB IRB6640 standard 6-axes robot, mounted on a 4.5 m linear axis. The layup head used is an 8 × 6.35 mm towhead (maximum bandwidth of 50.8mm). The compaction is performed by a suitable roller that guarantees a force of 500N, being the contact surface of the roller approximately 55mm × 15 mm. Therefore, the average applied contact pressure is around 0.6 MPa, being limited by the stiffness of the robot.
The programming of the panels was performed using Coriolis CAD-Fiber software. A 0.3 mm gap was programmed between courses, in order to avoid an overlap between tapes. An angular deviation of 3 degrees was set. A staggering of 22.2 mm (3.5 × ¼") was used between the plies, in order to avoid superposition of the inter-tape gaps. The heat source for processing thermoset prepreg materials is an 840W IR Lamp. The layup speed was 1.0m/s and the first ply was tacked by the machine on a bagging film.
Based on results achieved by theoretical models, a manufacturing test plan (Table 1) was defined to investigate two test cases, in particular two couples of panels layered up using AFPM followed by autoclave curing process. Carbon fiber/epoxy prepreg used in this project is the Cycom® HTA/977-2 from Cytec (Solvay Group) [Cycom, Cytec].

Test case	Panel ID	Size [mm]	Layup
A	#1	800 (0°) x 800	[+,-,0,90,+,-,0,90,+,-]s
	#1-opt	800 (0°) x 800	[0,90, OP, OP, OP, OP,+,-, OP,OP]s
B	#2	800 (0°) x 400	$[0]_{20}$
	#2-opt	800 (0°) x 400	[0,90, LO,RO, LO,RO,+,-, LO,RO]s

Table 1: Manufacturing Test Plan.

On one hand a standard quasi-isotropic layup sequence, panel #1, was compared with an optimized version, panel #1-opt (test case A); on the other hand a unidirectional layup sequence, panel #2, was compared with its optimized version, panel#2-opt (test case B). As reported in Fig. 12 (a and b), in the programming phase performed by CADFiber AFPM SW, due to manufacturing constraints, some assumptions to approximate the geodesic lines were made, in order to match the theoretical achievements.

3.3.2. *Mechanical tests and comparison with theoretical outcomes*

The above panels have been tested in laboratory. The Figure 12c shows the first experimental setup concerning the quasi-isotropic and optimized square panels.

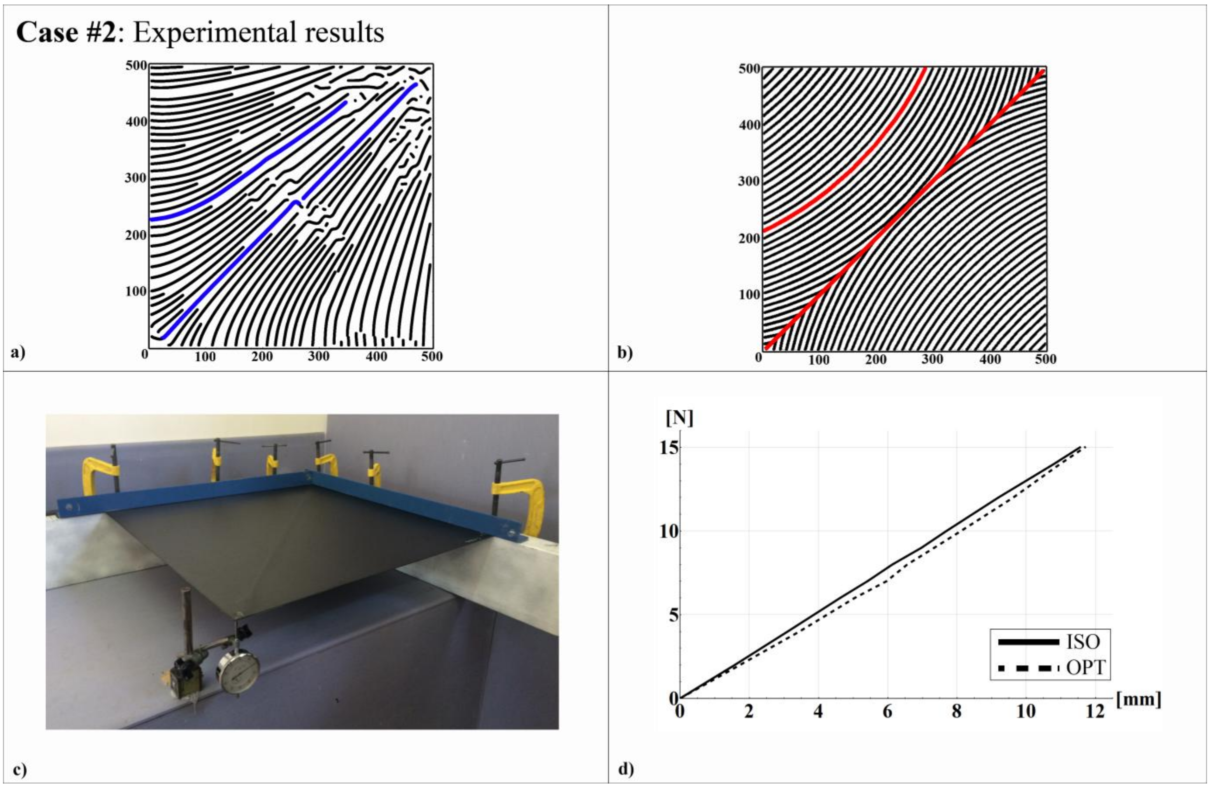

Fig. 12: Theoretically optimized fibers disposition (a); manufactured fibers disposition (b); mechanical test setup (c) and results (d).

Two adjacent sides have been constrained and the opposite angle has been loaded by a vertical force, up to 20N. A centesimal comparator has been used to compute the vertical displacements. The Figure 12 (d) shows the light difference between the quasi-isotropic and optimized displacements produced by the mechanical test. The maximum Strain Energy Gain is about 10%, very far from the numerical results (about 60%). This behavior can be related to the difficulty of the manufacturer to reproduce the theoretical distribution of the fibers, due to angular deviation, as showed in figure 12b.

The Figure 13 shows the second experimental setup, concerning the quasi-isotropic and optimized rectangular panels.

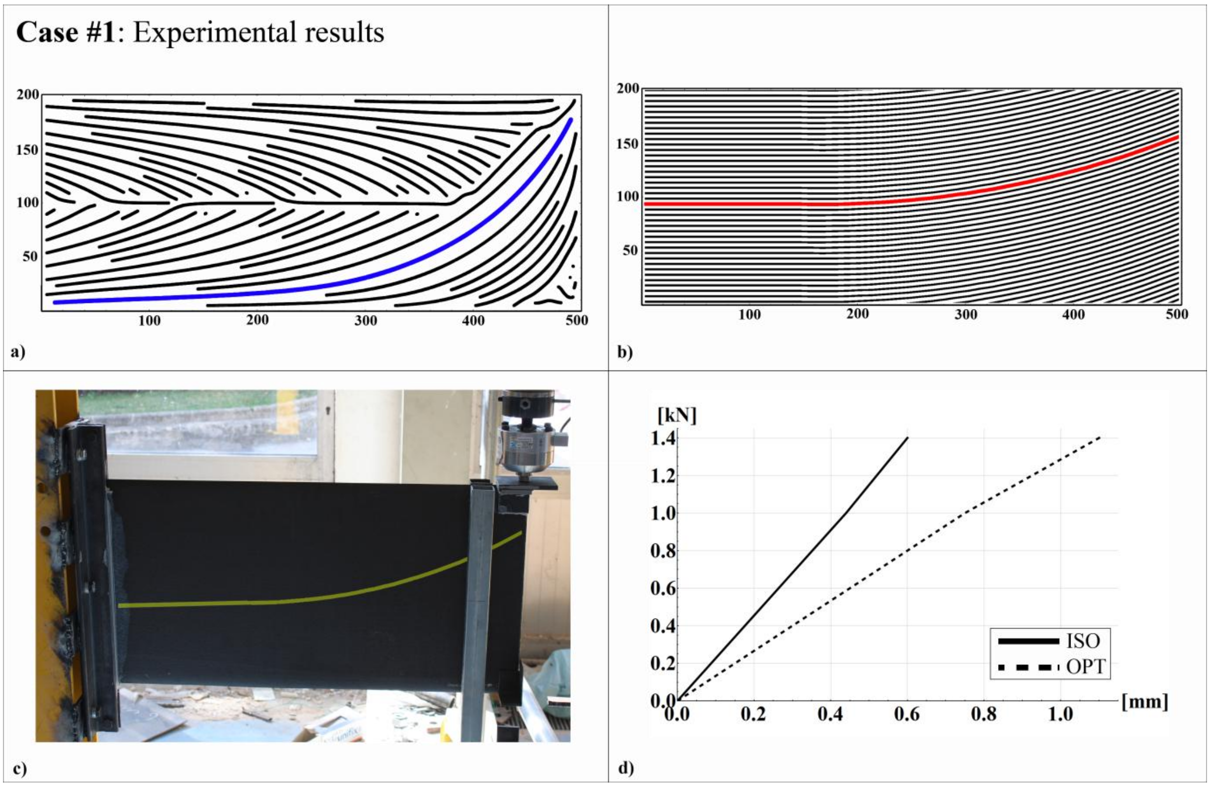

Fig. 13: Theoretically optimized fibers disposition (a); manufactured fibers disposition (b); mechanical test setup (c) and results (d).

The panels have been constrained on a short side and the upper opposite corner has been loaded by means of a vertical screw by means of a 10N load cell. Two parallel guides have been used to avoid lateral sliding. The Figure 13 (d) shows the strong difference between the quasi-isotropic and optimized displacements produced by the mechanical test. The average Strain Energy Gain is about 42%, no far to the numerical results (about 56%). Even in this case, the numerical gain is overestimated, due to the difference between the theoretical optimized fiber distribution and manufacturing one, as shown in Figure 13 (a and b).

4. Discussion and Conclusions

A mixed strain- and stress-based method for orthotropic FRCs, subject to either prescribed tractions or displacements, is proposed. Based on micromechanical approach, analytical solution has been presented, with regards to interlaminar stresses and strains. Finite Element analyses have been performed by means of a custom-made procedure, covering the analytical solution.

Several examples have been selected in order to verify the effectiveness of the proposed strategy, highlighting differences in terms of fibers optimization maps, related to boundary conditions. First example is paradigmatic: a rectangular panel in classical tension regime. The obtained optimal fibers orientation maps highlight the dual behavior of the structure; as expected, if the structure is subject to prescribed tractions, the fibers are oriented along the direction of loads, in this way maximizing the structural stiffness of the system. Dually, when the structure is subject to prescribed displacements, the optimal configuration provides fibers oriented along the minor direction of the structure, as well as orthogonal to the direction of the loading, in this way maximizing the structural compliance, i.e. minimizing the structural stiffness of the system.

In order to quantify the advantage obtained by the optimization procedure, neglecting or regarding to interlaminar stresses and strains, in the Table 2 results, in terms of the above-defined Strain Energy Gain, are summarized.

	Case Studies					
	#1	**#2**	**#3**	**#4**	**#5 (Rotations)**	**#5 (Torsions)**
Gain (± 1%)	**56.03%**	**61.35%**	**41.73%**	**19.23%**	**56.96%**	**55.12%**

Table 2: Strain Energy Gain.

In particular, the Strain Energy Gain seems to be quantitatively consistent, with maximum value upper than 60% for the case #2. The perceptual differences in terms of interlaminar stresses and strains remain negligible for the chosen structures, with a average value of one percent; however, a deeper investigation concerning post-elastic behavior is recommended in order to prevent delamination phenomena, as known, strictly related to interlaminar stresses and strains (Fraldi et al., 2014).

Finally, laboratory tests highlight how the theoretical Strain Energy Gains are overestimated, due to the difference between the theoretical optimized fiber distribution and manufacturing one, related to steering fibers angular deviation.

In conclusion, findings can be summarized as: i) a dual behavior is related to boundary conditions. If the structure is subject to prescribed tractions, the fibers are oriented along the direction of loads, in this way maximizing the structural stiffness of the system. Dually, when the structure is subject to prescribed displacements, the optimal configuration provides fibers oriented along the minor direction of the structure, as well as orthogonal to the direction of the loading, in this way maximizing the structural compliance, i.e. minimizing the structural stiffness of the system. ii) the optimization strategy furnish the same fibers distribution map for each layer of the composite ply; this behavior can be related to the fact that the interlaminar stresses and strains for the examined structures results two order of magnitude less than the plane stresses and strains. iii) the strain energy gains result substantially equal (with a average value of one percent) with neglecting or regarding to interlaminar stress and strain, because delamination phenomena, strictly associated to interlaminar stresses and strains, are related to post-elastic behavior. iv) laboratory tests highlight how the theoretical Strain Energy Gains are overestimated, due to the difference between the theoretical optimized fiber distribution and manufacturing one, related to steering fibers angular deviation.

References

Barbero J. 1999. Introduction to composite materials design. Taylor & Francis.

Barbero J. 2008. Finite element analysis of composite materials. CRC Press.

Bendsøe MP, Kikuchi N. 1988. Generating optimal topologies in structural design using a homogeneization method. Comput. Methods Appl. Mech. Eng. 71:197-224.

Bendsøe MP, Sigmund O. 2003. Topology Optimization-Theory, Methods and Applications. Springer, Berlin.

Bendsøe MP. 1989. Optimal shape design as a material distribution problem. Struct Optim. 1(4): 193–202.

Brampton CJ, WU KC, Kim HA. 2015. New optimization method for steered fiber composites using the level set method. Struct Multidisc Optim. 52:493–505.

Bruyneel. 2011. SFP-a new parameterization based on shape functions for optimal material selection: Application to conventional composite plies. Struct Multidisc Optim. 43(1):17-27.

Cheng HC, Kikuchi N. 1994. An improved approach for determining the optimal orientation of orthotropic material. Struct Optim. 8:101-112.

Cheng HC, Pedersen N. 1997. On sufficiency conditions for optimal design based on extremum principles of mechanics. J. Mech. Phys. Solids. 45:135-150.

Diaz AR, Bendsøe MP. 1992. Shape optimization of structures for multiple loading conditions using a homogenization method. Struct Optim. 4:17-22.

Duysinx P, Bendsøe MP. 1998. Topology optimization of continuum structures with local stress constraints. Int J Numer Methods Eng. 43:1453-1478.

Eschenauer HA, Olhoff N. 2001. Topology optimization of continuum structures: a review. Appl Mech Rev. 54:331-389.

Foldager J, Hansen JS, Olhoff N. 1998. A general approach forcing convexity of ply angle optimization in composite laminates. Struct. Optim. 16:201-211.

Fraldi M, Cutolo A, Esposito L, Perrella G, Pastore Carbone MG, Sansone L, Scherillo G, Mensitieri G. 2014. Delamination onset and design criteria of multilayer flexible packaging under high pressure treatments. Innovative Food Science and Emerging Technologies. 23:39-53.

Gao T, Zhang W, Duysinx P. 2012. A bi-value coding parameterization scheme for the discrete optimal orientation design of the composite laminate. Int J Numer Methods Eng. 91(1):98-114.

Gea HC, Luo JH. 2004. On the stress-based and strain-based methodsfor predicting optimal orientation of orthotropic materials. Struct Multidisc Optim 26:229-234.

Gurdal Z, Omedo R, 1993. In-plane response of laminates with spatially varying fiber orientations: Variable stiffness concept. AIAA J. 31(4):751-758.

Klarbring A, Stromberg N. 2012. A note on the min-max formulation of stiffness optimization including non-zero prescribed displacements. Struct Multidisc Optim. 45:147-149.

Luo JH, Gea HC. 1998. Optimal orientation of orthotropic materials using an energy based method. Struct. Optim. 15:230-236.

Pedersen N. 1989. On optimal orientation of orthotropic materials. Struct. Optim. 1:101-106.

Pedersen N. 1990. Bounds on elastic energy in solids of orthotropic materials. Struct. Optim. 2:55-63.

Pedersen P, Pedersen N. 2011. Design objectives with non-zero prescribed support displacements. Struct Multidisc Optim. 43:205-214.

Raju G, Wu Z, Weaver PM. 2012. Prebuckling and buckling analysis of variable angle towplates with general boundary conditions. Compos Struct. 94(9):2961-2970.

Rovati M, Taliercio A. 2003. Stationarity of the strain energy density for some classes of anisotropic solids. Int. J. Solids Struct. 40:6043-6075.

Rozvany GIN, Zhou M, Birker T. 1992. Generalized shape optimization without homogenization. Struct. Optim. 4:250-254.

Stegmann J, Lund E, 2005. Discrete material optimization of general composite shell structures. Int. J. Numer. Methods Eng. 6:2009-2027.

Sigmund O, Torquato S. 1997. Design of materials with extreme thermal expansion using a three-phase topology optimization method. J Mech Phys Solids. 4:1037–1067.

Suzuki K, Kikuchi N. 1991. A homogenization method for shape and topology optimization. Comput. Methods Appl. Mech. Eng. 93:291-318.

Tatting B, Gürdal Z. 2001. Analysis and design of tow-steered variable stiffness composite laminates. In: American helicopter society Hampton Roads chapter, structures specialists' meeting.

Tosh MW, Kelly DW. 2000. On the design, manufacture and testing of trajectorial fiber steering for carbon fiber composite laminates. Compos Part A. 31:1047-1060

Wu KC. 2008. Design and analysis of tow-steered composite shells using fiber placement. American Society for Composites. 23rd Annual Technical Conference Memphis. Sept 9-11.